OK, so the computer has understand, what about me?
Eugene Wigner, Nobel Laureate

The succeeding material is structured as follows:

1. Isolated broadband linear polarized (LP) back-fed stacked U-slot patch radiator and its CST MWS numerical simulation with the discussion of the results. This case is classified as no-mutual coupling environment.
2. The same radiator in an infinite array environment and the CST MWS numerical simulation using the periodic boundary conditions with the discussion of the results.
3. A finite array of 5x16 elements in a rectangular lattice.
4. A finite array of 5x16 elements in a triangular lattice.
5. Comparative analysis. The main objective of such a study is to minimize the embedded antenna database of 5G phased array platform/wizard and provide some recommendations to obtain consistent results.

Keep in the mind this section is currently in development. Please come back from time to time to follow the latest update.

Come back tomorrow to check for the update.

Section 1. Isolated broadband linear polarized (LP) back-fed stacked U-slot patch radiator.

Figure 1 depicts the CST model of the proposed radiator optimized for 24 – 30 GHz band. The radiator is compact, low profile, easy-to-integrate, lightweight, low cost, and quite simple to provide fast numerical simulation. The combination of two resonant components, a fed patch with a stacked element and U-slot, yields dual broadband characteristics (see J.A. Anasari and R. B. Ram, "Broadband Stacked U-slot Microstrip Patch Antenna, *Progress In Electromagnetics*

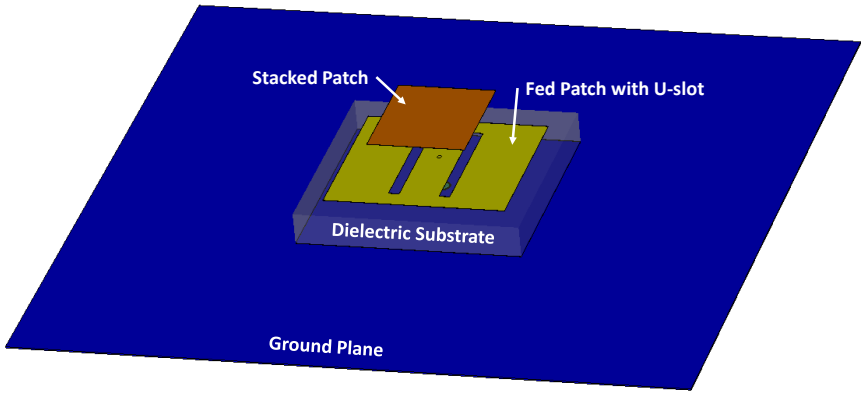

Figure 1. CST model of a single radiator on the large PEC ground plane

Research Letters, Vol. 4, pp. 17–24, 2008) that are required in 5G systems with high data rate and low latency.

The back-fed U-slot is connected to a generator through 50 Ohm coaxial connector as Figure 2 demonstrates. Figure 3 and 4 below present the radiator schematics with all dimensions in mm.

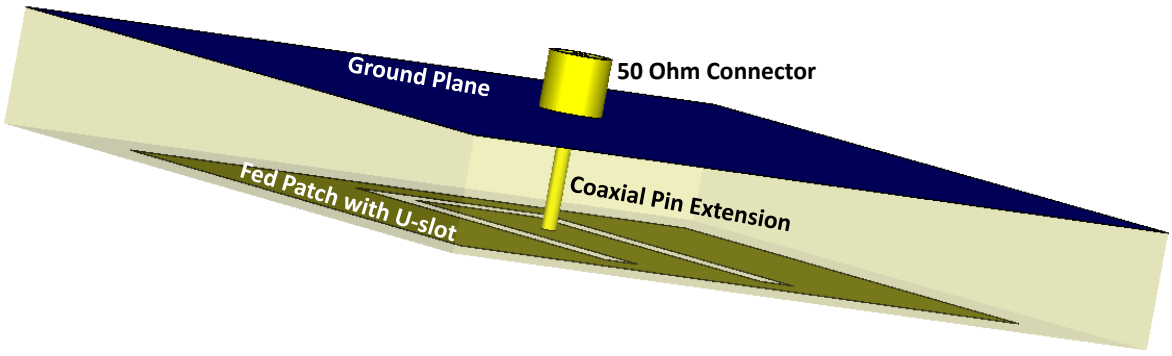

Figure 2. Coaxial connector connected to fed patch with U-slot

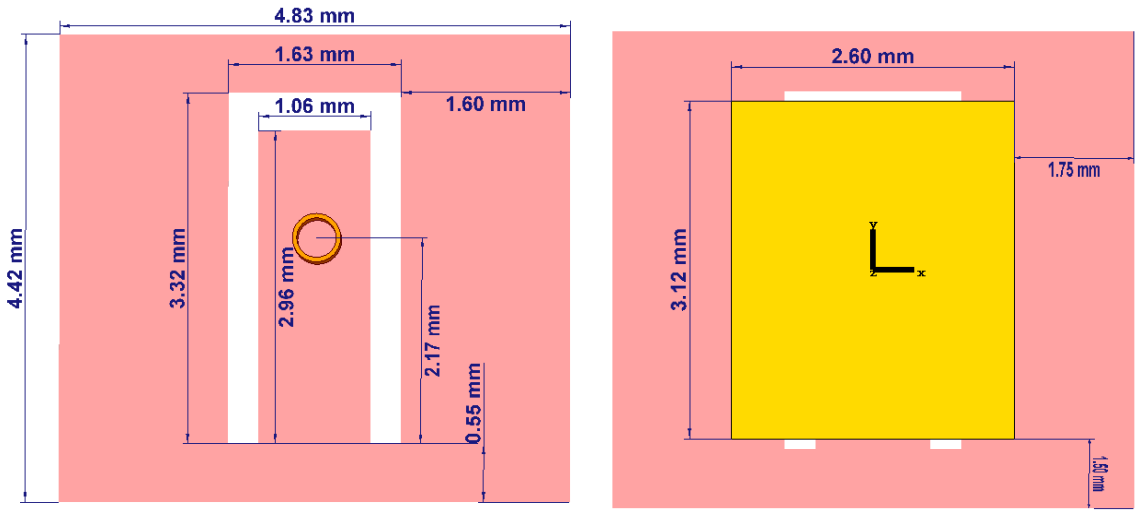

Figure 3. Element schematics. Top view of fed patch (left), U-slot and fed and stacked patch (right)

The side arms of U-slot are symmetrically positioned with respect to the coax feed point being shifted on 0.34 mm relative to the origin. The thin dielectric substrate of ultra-low permittivity of 1.07[1] assurances the least possibility of surface waves. The stacked patch might be supported by a dielectric rod of small diameter (not shown in the drawing) or an additional layer of the same dielectric. The radiator model was developed using 3D full-wave CST MWS software and simulated in the time domain to get the wideband data over just one run. The frequency response

[1] For example, ROHACELL® 51 IG/A with tan δ = 0.0037 that can are foamed into a finished core in a mold with all patches directly integrated during the foaming process. See https://www.rohacell.com/sites/lists/re/documentshp/rohacell-dielectric-properties-en.pdf and https://www.rohacell.com/product/rohacell/en/downloads/press-releases/pages/article.aspx?articleId=101326.

is obtained through a Fast Fourier Transform (FFT) afterward. Since the time domain simulation is performed on a port-by-port basis, it takes less memory and faster as compared to the frequency domain. To reduce the back-lobe radiation and effect of metal edge diffraction, the ground screen was extended to 18x18mm. That is about extra 6 mm from each side of the fed-patch and slightly more than half of the wavelength at 30 GHz.

If you intend to rerun the CST project on your computer, go to URL https://1drv.ms/f/s!AjtsKS-uvNP1j2bBbNiMEMrekiFo, click the right mouse button on the icon **Single24GHz.cst**, and choose the option Download. Save this file anywhere on your computer and then run Single24GHz.cst project. Keep in mind that the model was developed using CST STUDIO SUITE, Version 2017.00.

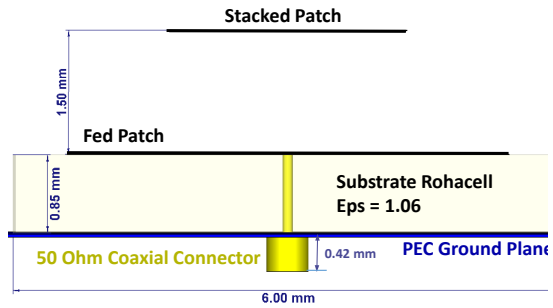

Figure 4. Element schematics. Side view

The same way you can copy, store, and import .stp and .hlg files if your full-wave software is ANSYS HFSS or any other toolbox. Need different file format. Live the message on the Contact page of https://emfieldbook.com.

Figure 5 reflects the radiator return loss over the frequency marked as 'S11, Radiator'. The enclosed picture is the proposed lumped equivalent circuit of the radiator and its return loss characteristic marked as 'Equivalent Circuit.' CST file S11.txt and Matlab script

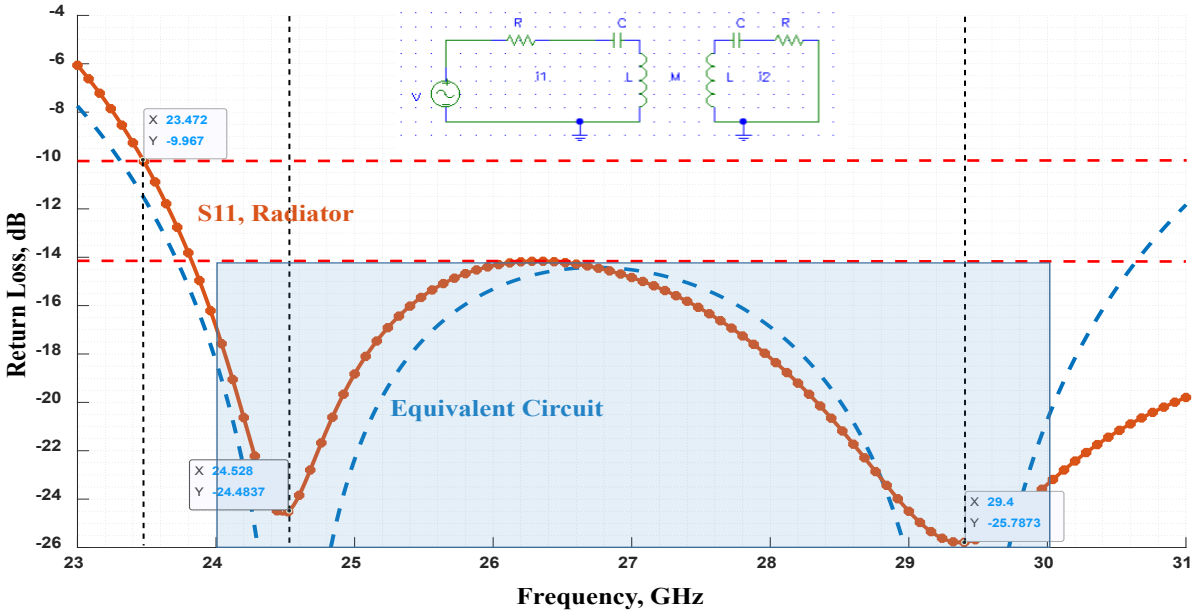

Figure 5. Return loss of radiator and its lumped equivalent circuit vs. frequency

CoupledResonances.m to read and plot this figure can be found at the URL mention above. According to Figure 5 and Smith chart in Figure 6, there are two resonances, one around 24.53GHz

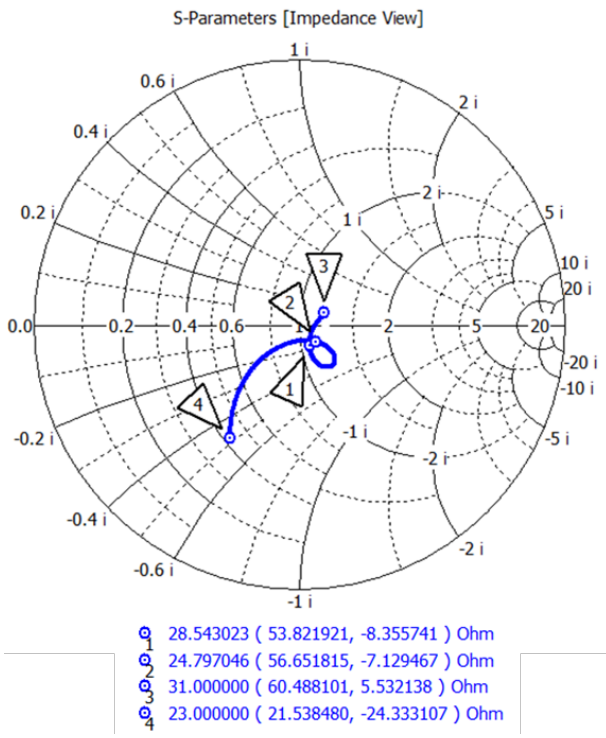

Figure 6. Normalized to 50 Ohms Input Impedance of radiator

and the other close to 25.4GHz, where the return loss reaches its minimums, i.e., at

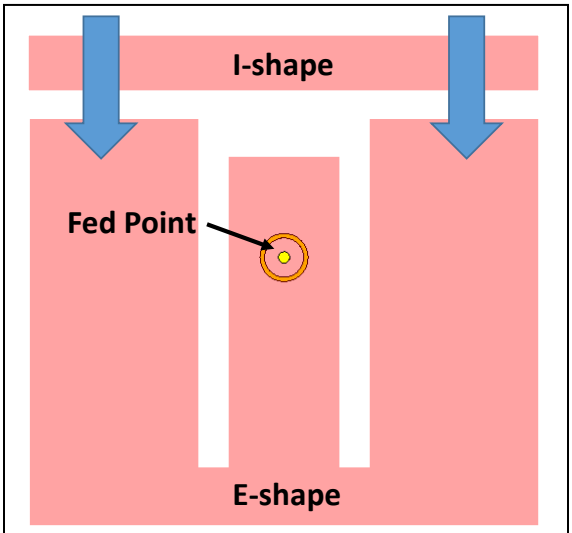

Figure 7. Fed patch with U-slot as the composition of E- and I-shape metal traces.

those frequencies the accumulated nearby the radiator E-field energy $W_e \cong W_m$ (see VJ[2], pp.139 – 142) where W_m is the accumulated nearby H-field energy. The simple explanation follows from E- and H-field structure nearby the fed patch of E-shape microstrip with I-shape trace on the top as Figure 7 shows. The fed by coax interior vertical element of E-shape has the length of 2.96mm (check Figure 3) and can be considered as the $\lambda/4$ - resonator on a dielectric substrate of $\varepsilon = 1.06$ at the frequency 24.6 GHz that is very close to the shown resonance at 24.53GHz. The additional shift of about 100MHz is due to the concentration of E-field energy mostly in the gap between the resonator edge and I-shape element. Eventually, that is the equivalent to capacitance[2] pulling down the resonance frequency. Supporting this statement E- and H-field structures along the slot are depicted in Figure 8 and 9 at close to resonance 24 GHz. The second resonance at 29.4GHz is supported by standing wave forming along E-shape between the coaxial probe and shorted end. Since the high concentration of H-field energy W_m nearby electrical current over the pin corresponds to some parallel inductance[2] , the physical separation of 2.17mm (see Figure 3) between the probe and E-shape shorted end should be slightly less than $\lambda/4 = 2.55$mm. Figure 10 demonstrates the distribution of the surface electrical current on the fed patch at 29GHz that is generated by the probe. According to this drawing, the current and excited by it H-field extends beyond the probe, thereby increasing the resonator electrical length up to the required 2.55mm. Therefore, the characteristic in Figure 5 is formed by the interaction between two resonance circuit inductively coupled by common H-fields that is mainly locked around the central element of E-shape.

[2] Read Section 3.1.11 Concept of Capacitance and Section 3.1.12 Concept of Inductance, V.I. Volman and A. Jeziorski, Engineering Electrodynamics, pp. 126 -129. **The subsequent references to this book are denoted as VJ.**

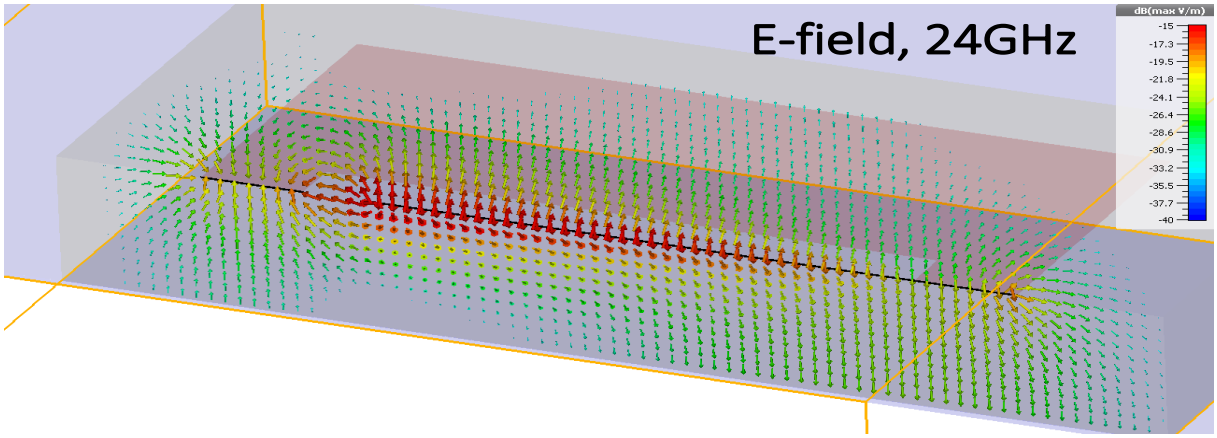

Figure 8. E-field reaches the maximum inside the gap

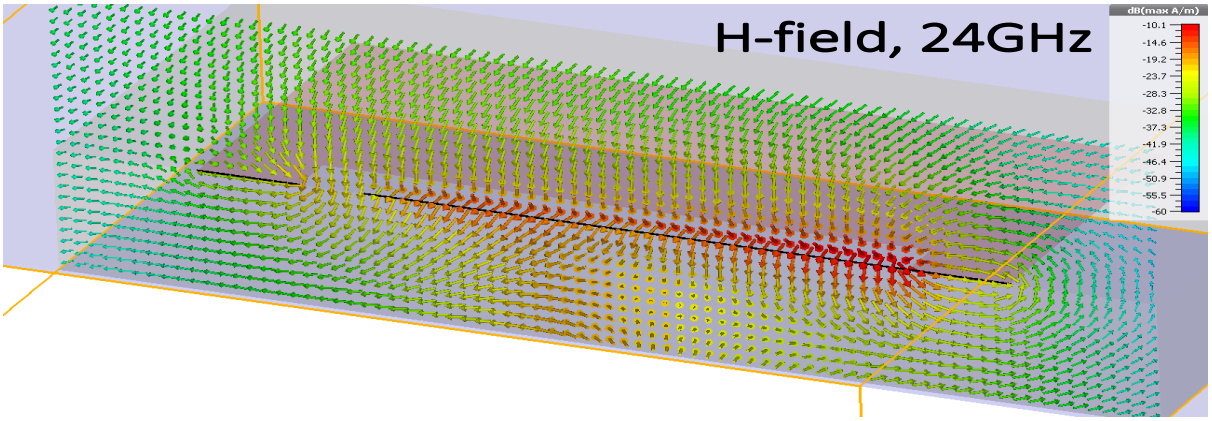

Figure 9. H-field reaches the maximum at cross section where the resonator is shorted.

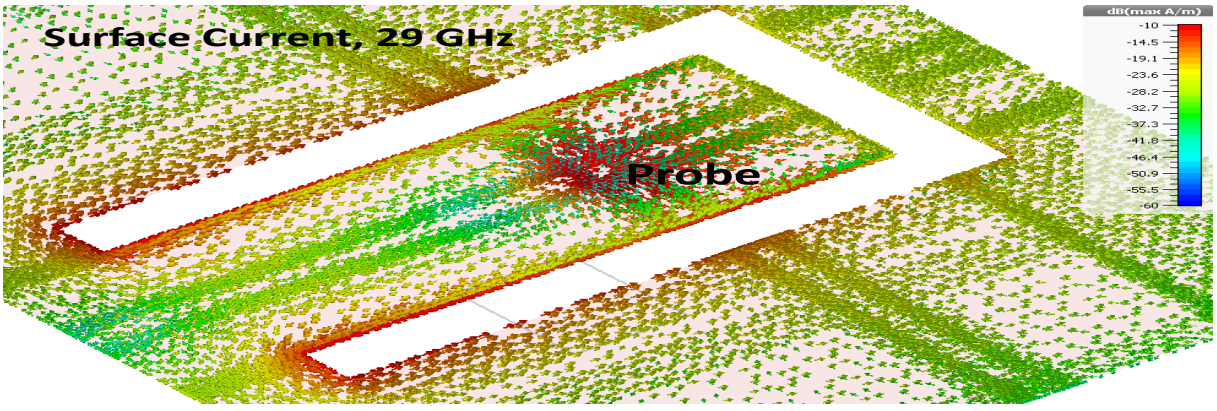

Figure 10. Surface electrical current distribution on the patch at 29GHz.

Excellent matching performance (bellow -14 dB, light blue area in Figure 5) and tiny radiator sizes cause its high radiation and total efficiency. Remind that the radiation efficiency reflects just Ohmic loss while the total includes Ohmic and mismatch loss.

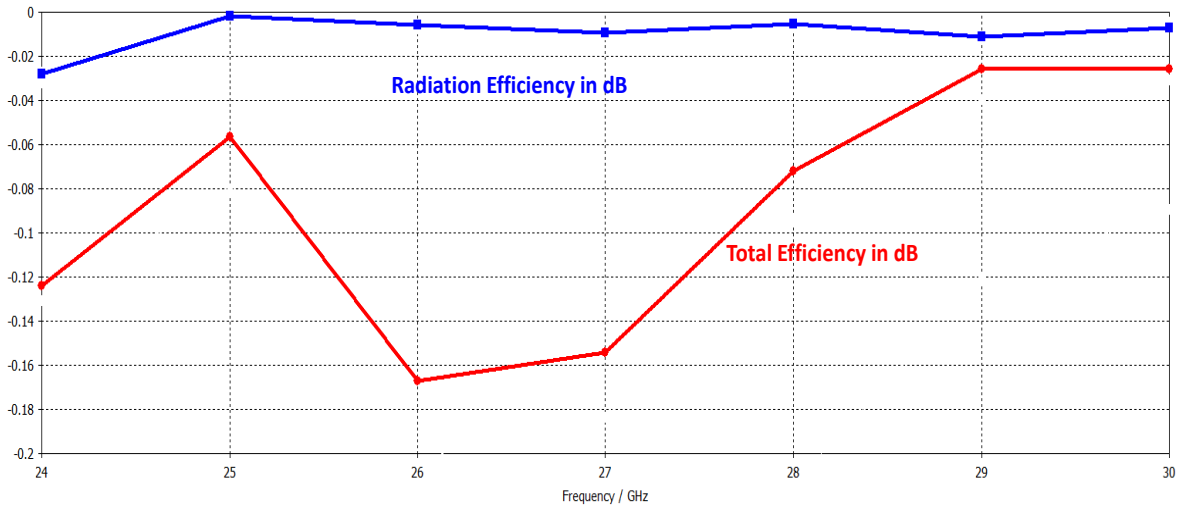

Figure 11. Radiation and Total Efficiency.

Let's make several remarks about the stacked patch role. The radiator input impedance vs. frequency without this patch presented in Figure 12. The reflection coefficient $|\Gamma| \leq 0.4$ or VSWR ≤ 2.33 that just slightly exceeds generally required level VSWR $= 2$. The shape of curve looks like similar to shown in Figure 6, but now the input impedance has quite significant capacitive component meaning that E-near-field reactive energy around the fed patch surpasses the reactive energy accumulated in H-near-field (check the reference[2] above). Just compare the left and right images in Figure 13, indicating this fact at 27GHz.

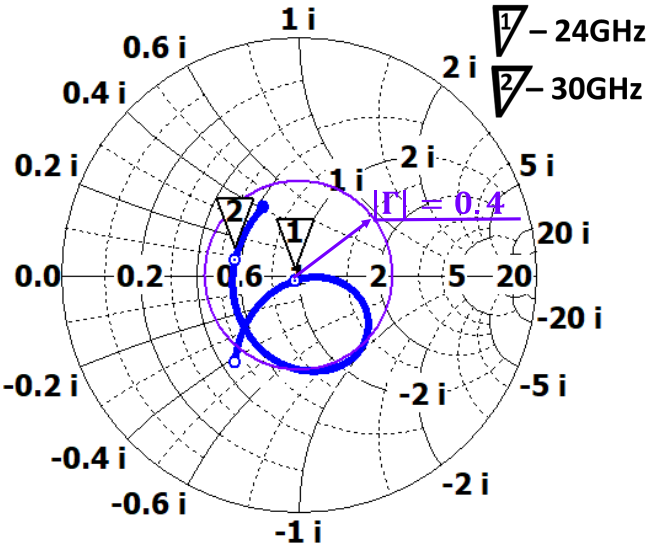

Figure 12. Normalized to 50 Ohm Input Impedance of radiator without the stacked patch.

Meanwhile, according to Figure 3, the sizes of the stacked patch are 3.12x2.60 mm, i.e., far less than $\lambda/2$ at any in-band frequency. If so, it works as a section of an open-circuit line capacitive by nature. Since the separation between the patch and coaxial port is 1.55mm + 0.85mm + 0.42mm = 2.77mm (see Figure 4), i.e., approximately $\lambda/4$ at 27GHz, this capacitance transforms into inductance, as expected, thereby reducing the misbalance between electric and magnetic energy, i.e., keeping $W_e \cong W_m$ at in-band frequencies.

Hopefully, such tight connections between the lamp circuitry interpretation and radiator performance might pave the way to the radiator synthesis.

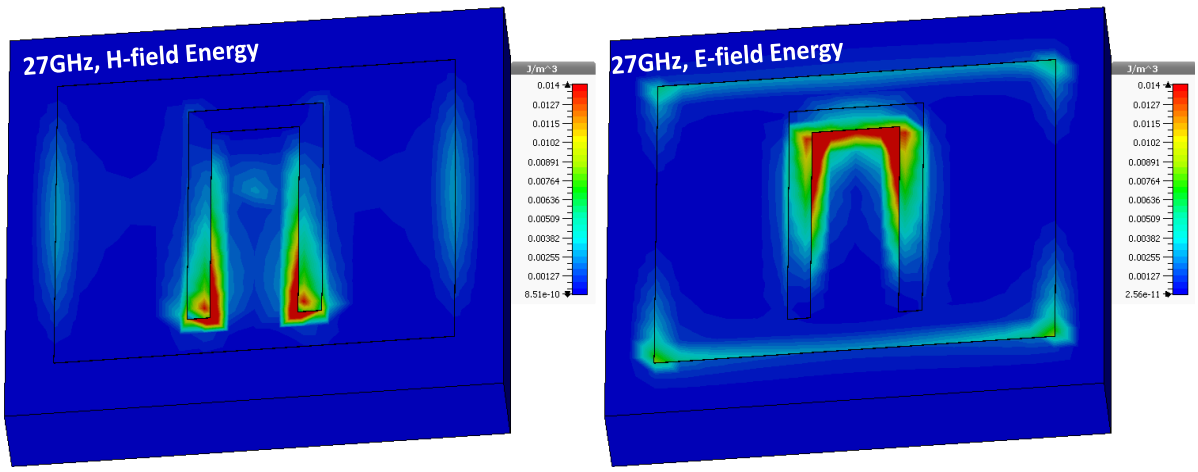

Figure 13. H- and E-field energy distribution over the fed patch at the middle of band. The peak energy is the same on both images and equal to 0.014 J/m^3.

Figure 14 depicts the radiator patterns and demonstrates almost constant directivity around 9 dBi through the band frequencies. CST simulation indicates that the **elimination** of the stacked patch

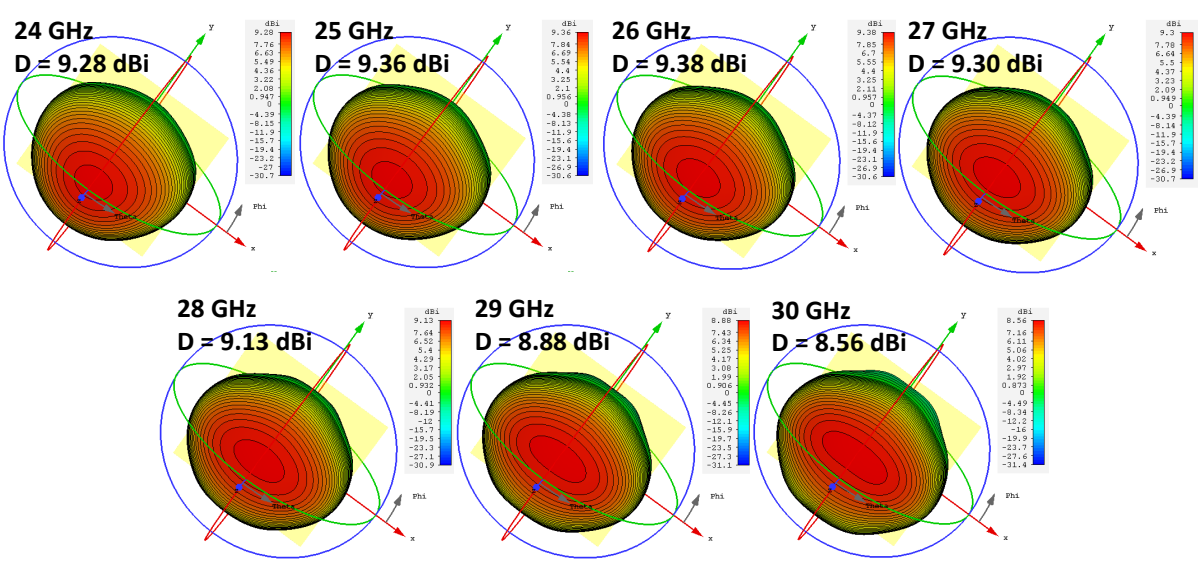

Figure 14. Radiator patterns

increases moderately the radiator directivity from 0.04 dB up to 0.40 dB depending on frequency (To check it open **Single24GHz.cst** project in CST STUDIO SUITE, click the right mouse on the line 'stacked' inside 'component1' block of Navigation Tree on the left, choose the option 'Change Material and Color', designate 'Material' as vacuum, and rerun project). Therefore, the leading role of this patch is the matching do-gooder.

Section 2. The same radiator located in a periodic array with an infinite number of elements.

First of all, several words about a periodic array definition. The schematic of a 2D infinite planar array in a rectangular lattice is presented in Figure 15. Each element position is marked by cross-symbol. Since the separation between any adjacent elements is equal, the array possesses the translation symmetry. The latter means that any of radiators fits exactly onto itself being translated a given distance, i.e., *m*dx* or *n*dy* or both simultaneously where *m* and *n* are positive or negative integers. It should be expected and is accurate that the same translation symmetry possesses the nearby E- and H-fields emitted by the array. Based on this idea Floquet–Bloch theory allows reducing the computation problem to the study of a unit cell with properly formulated boundary conditions reflecting the array periodicity (look through Section 31.6, Figure 31.7, and equation (31.91) in Modern Antenna Handbook, Jon Wiley & Sons, 2008, edited by Constantine A. Balanis). Roughly speaking, a radiator in such array unit has infinite, i.e., the same number of neighbors and thereby the same interaction level aka mutual coupling with neighbors. As a result, every element has the same pattern, and the so-called *scan input impedance.* We use this term to define the input impedance of each antenna element when all of them are excited uniformly in magnitude and progressively in phase while the antenna main beam is steered. Figure 16 reflects the damaging role of mutual coupling.

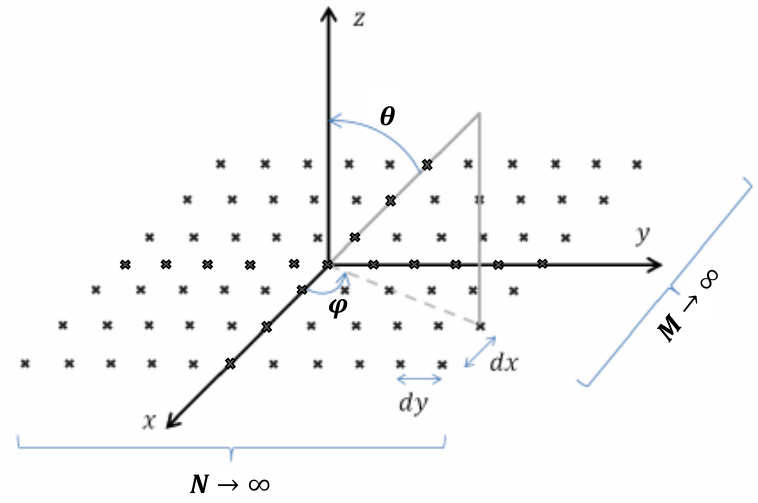

Figure 15. Schematic of infinite array in rectangular lattice

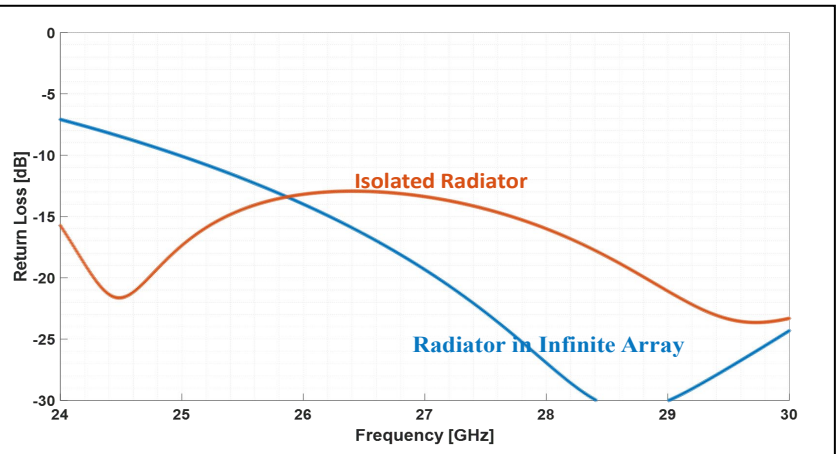

Figure 16. Return Loss of isolated and the same radiator in infinite array emitting boresight

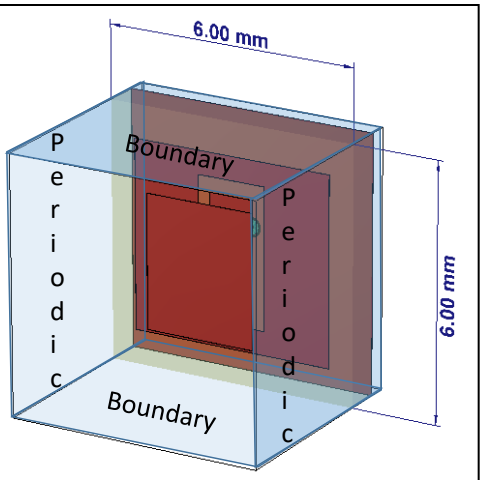

Figure 17. Element schematic in infinite-array environment

The resonance at 24.5GHz wholly dissipated, the resonance at 29.4GHz shifted down in frequency, and -10 dB bandpass shrinks drastically. Such deviations are understandable because the mutual coupling means, in reality, changing the structure of E- and H-fields nearby the radiator and breaching the balance between them.

Figure 17 demonstrates the schematic of the CST model with periodic boundary box of 6 x 6mm. It indicates that in Figure 15 $dx = dy = 6$mm and the possibility to meet the antenna packaging compactness. To get all results, copy file **Periodic24GHz.cst** from URL https://1drv.ms/f/s!AjtsKS-uvNP1j2bBbNiMEMrekiFo, store it and run on your computer.

The discussion in Section 1 paves the way how to fix the harm of the mutual coupling. The first resonance was returned in-band by lengthening the interior vertical element of E-shape, increasing on 1mm the separation between the fed and stacked patch, and slight scaling the fed-patch. The final CST file **FinalPeriodic24GHz.cst** can be found going to the URL mentioned above. Figure 18 illustrates the radiator return loss after all tuning. It not as broadband as shown in Figure 5 but

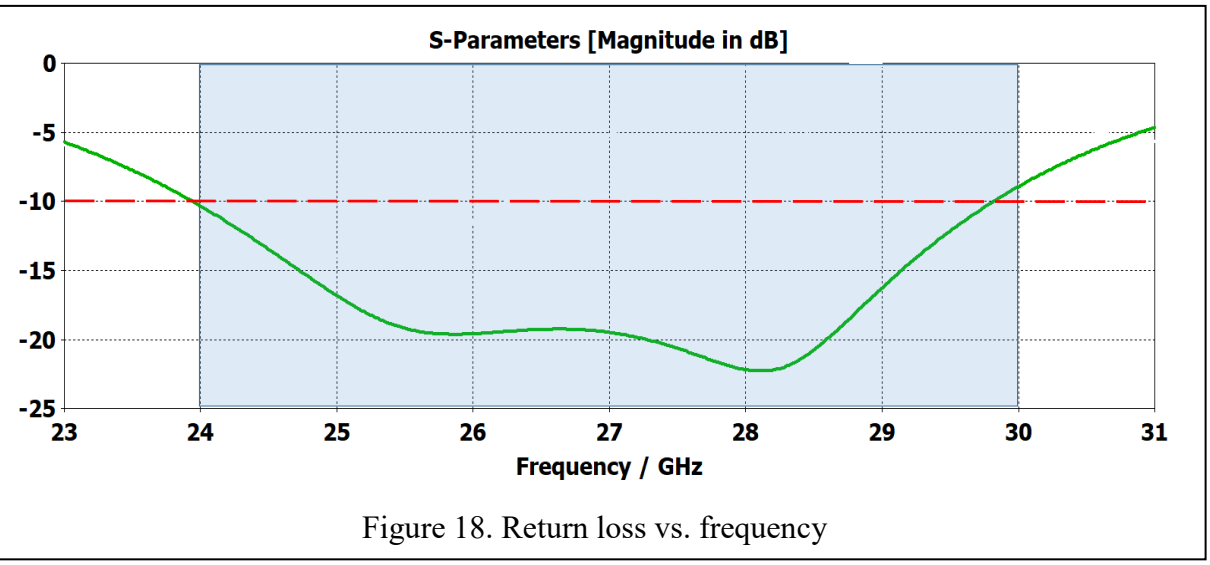

Figure 18. Return loss vs. frequency

however covers two 5G adjacent sub-bands. Figure 19 depicts the radiator patterns and demonstrates almost constant directivity around 6 dBi through the band frequencies. Compare these plots and shown in Figure 14. The shape of the patterns is indeed very similar, but how to explain the directivity dropping between 2 dBi and 4.2 dBi. Plainly, each adjacent element in the infinite array is not only emitted energy from its generator but works as a receiving antenna (see Section 3.4.3 Lorentz's Reciprocity Theorem in VJ, pp. 155-161)) absorbing the energy from surrounding elements. As a result, the effective aperture (see VJ, pp. 223 – 225) of element in infinite array generally shrinks to the single-cell aperture as the separations *dx* and *dy* are not above

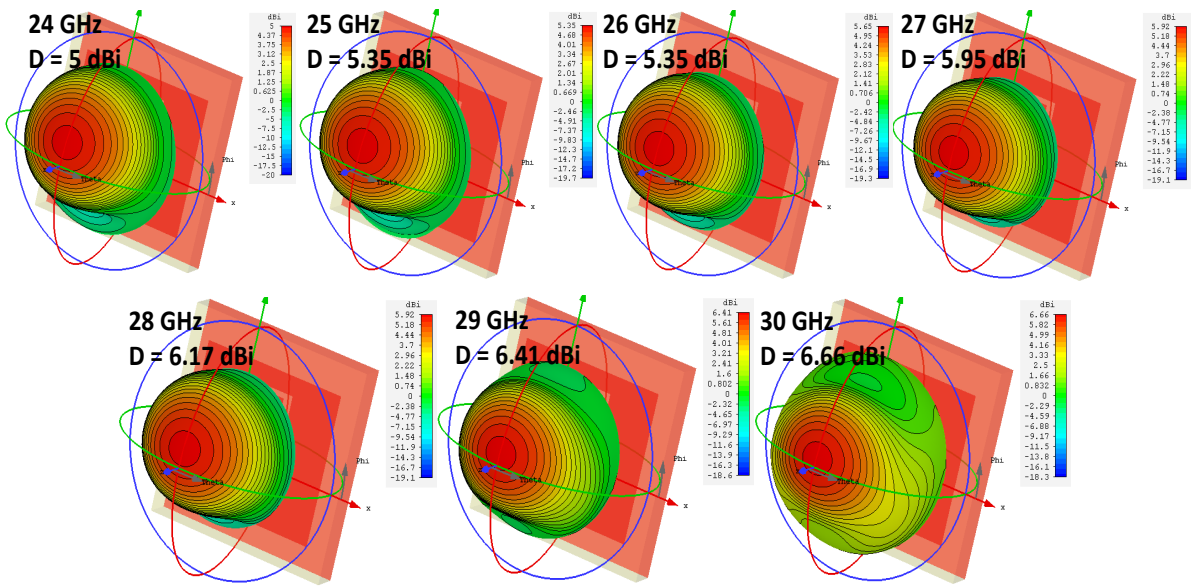

Figure 19. Radiator patterns

(0.5 – 0.65) λ. If so, the directivity of a radiator in infinite array of such density does not exceed $D = 4\pi A_{cell}/\lambda^2$ or $D = \pi$ (~5dBi) as soon as $A_{cell} = 0.5\lambda * 0.5\lambda = 0.25\lambda^2$. The full-wave simulation supports this explanation relatively fine. Figure 19 pictures the normalized to the peak magnitude (in dB) distribution of the tangential components of E- and H-fields over the plane of 7mm above two radiators' substrate. One of them is the central element in 5x16 array panel (element #40 in Figure 1 of Section 5 below). It is a well-suited model of a radiator in infinite-array environment revitalizing the fields in a much wider area than cell in Figure 17. The second spreading corresponds to the isolated (see Figure 1 in Section 1) element with the ground plane of

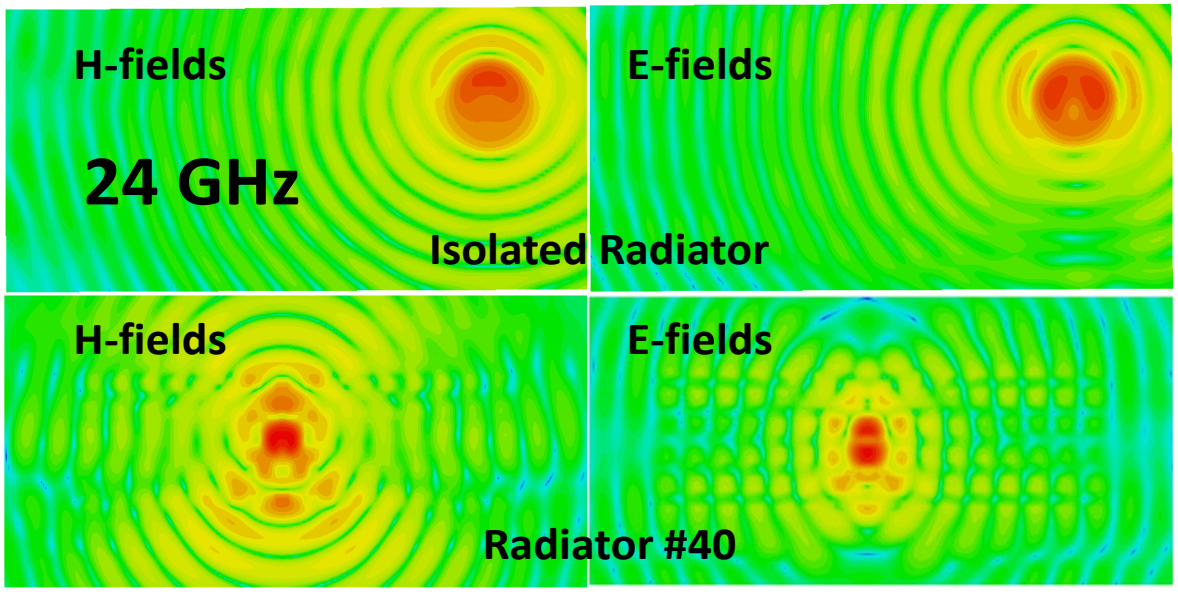

Figure 20. E- and H-field distribution.

the same sizes as the array panel to keep the correct geometrical and magnitude scale. The images speak for themselves and do not require additional comments. The chosen frequency is 24GHz, where the drop in directivity is highest and equal to 4.28 dBi.

5G base station antenna array besides to be broadband should support the array beam steering within a field-of-view up to ±45° in azimuth and ±15° in elevation. That allows reducing interference by dynamically scan antenna beams away from intrusive sources and steering maximum of RF beams energy in the direction of customers. Figure 21 demonstrates the

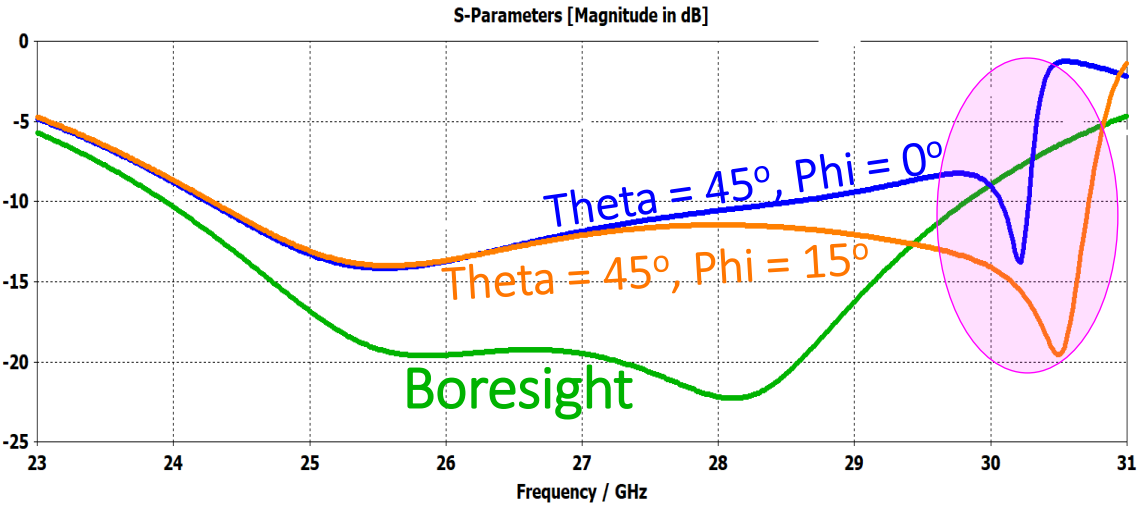

Figure 21. Scan performance. Return Loss in dB

broadband scanability of the optimized array element. Wild variations of return loss above 29GHz are predictable and correspond to frequencies band (pink oval) where the grating lobe is expected.

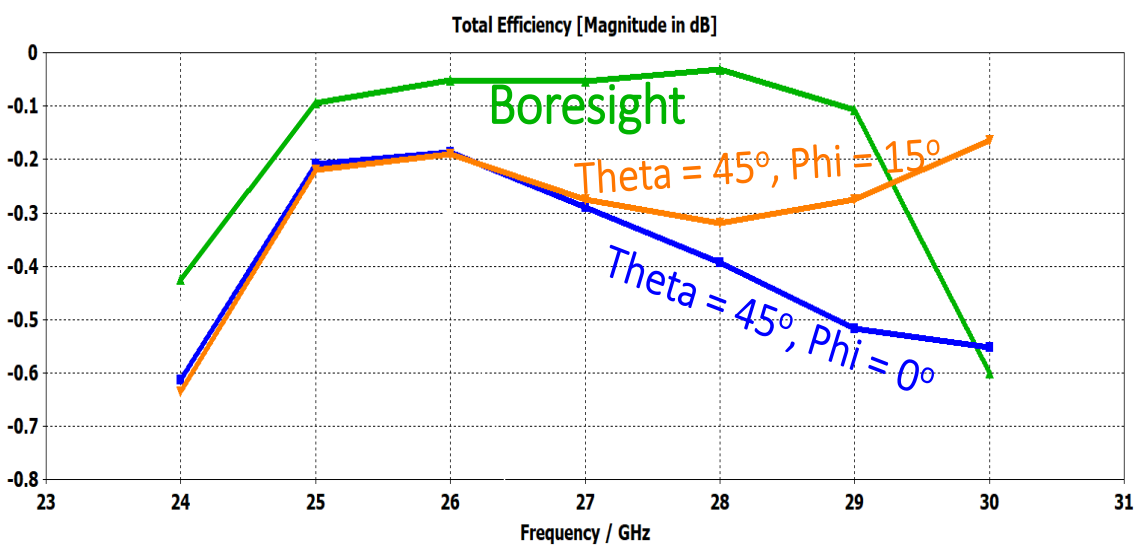

Figure 22. Total Efficiency in dB

The total element efficiency, i.e., Ohmic + Mismatch loss, is presented in Figure 22 and can be seen as pretty good.

Come back tomorrow to check for the update.

Sections 3-5. Comparative analysis

24 – 30 GHz Phased Array for 5G Network Base Station

This article discusses and compares different ways of 5G phased array platform/wizard development and provides some recommendations to obtain consistent results.

The phased antenna array is one of the lead front-end components of current and coming 5G communication systems that defines their massive MIMO performance. The trend outlined in recent years is to provide "… a robust and complete platform/wizard for RF/microwave engineers … " to "… develop … more capable antenna and other RF front-end components in less time as before." [1]. "Benefits of systems operating at mmWave frequencies include the small sizes of antennas and the larger available bandwidth" [2]. Regrettably, a wide variety of application-driven requirements (city or rural environment, a realized gain, scan and polarization performance, impedance matching, etc.) cannot be met by single and forever designed element. It means that any practically convenient model platform/toolbox must contain an extensive library of predesigned antenna elements. Misfortunately, 5G antennas belong to a class of relatively small and densely populated phased arrays where the total number of radiators typically does not exceed several hundred. If so, the consistency of results obtained through such system-level platform ultimately depends on the correctness of the phased array elements' model that should include the relatively strong (-15dB or 0.18V relative to 1V element excitation and sometimes even higher) mutual coupling with other elements in the array. We will demonstrate below that the presence of mutual coupling in such arrays noticeably modifies the elements' input impedance, distorts the shape of their pattern making it wider and asymmetrical, splitting the main beam, shifting the direction of peak radiation, etc. The most alarming that such distortions depend on the radiator position in the array. Indeed, look at Fig. 1. Each of the *rim* elements marked in red is lacking of neighboring elements from one of its side. Each of the *next-to-rim* elements enclosed in blue rectangles is under the influence of rim neighboring elements from one side and multiple inner elements. Finally, each of the *center* elements has symmetrically populated 2 layers of neighbors. Therefore, each of 36 rims + 32 close to rim elements (~ 85% (!)) should display the unique performance relative to the center elements. Note that even in an array of 32x32 = 1024 radiators the number of such elements is 248 or 24.2%. Therefore, we can expect that the array likes shown in Fig.1 could be divided into groups of several elements with comparable performance letting highlight a typical representative inside each group. The following analysis

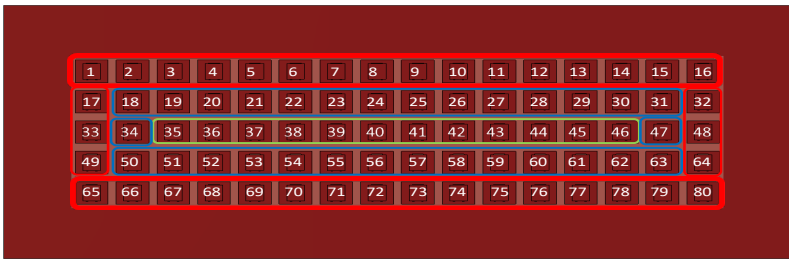

Figure 1. 5x16 array planar panel

demonstrates that the array of 4x4 sizes and more may be designed based on just 3 elements, one from row 1 or 5 as the representative of rim elements, one from row 2 or 4 as the representative of next-to-rim elements, and one from row 3 as the representative of all elements between rim and next-to-rim rows. Thereby, the embedded library database could be truncated without sacrificing the correctness of final results actually. According to [3], "… the power consumption of a 5G station is *three times* that of its 4G LTE predecessor." If so, each dBi error in the assessment of array gain may be quite costly.

To date, the antenna array block of numerous platforms bypasses the difficulties using either data from single radiator simulation/test in free space (it means all elements are identical and mutual coupling is ignored) or low complexity and memory consumption Floquet-Bloch technique. The later assumes that all radiators are set in an *infinite* array and thus identical once again since each element is mutually coupled with the same *infinite* number of driven neighbors. We will demonstrate why both approaches have limited accuracy and how to overcome them.

The paper is divided into several sections, starting in Section 1 the discussion of the mutual coupling and grating lobe as the critical issues in beam steering phased array. In Section 2, the schematic of the broadband patch element appropriate for practical applications is presented. Section 3 demonstrates the CST MWS + Matlab simulation results[3] as soon as such element is placed into the environment of the infinite periodic array. Section 4 and 5 present the results of the full-wave CST simulation of 5x16 array based on the same element, while Section 6 discloses the CST analysis results of the same array, but in a triangular lattice. The investigation outcome is summarized in the Conclusions.

1. Mutual Coupling and Grating Lobe in Beam Steering Phased Array

Before starting the analysis note that the total interaction between elements might be loosely divided into 3 categories; spatial proximity, aperture coupling, and surface wave interaction. More or less, the proximity interaction is defined by nearby quasi-static E- and H-fields. For microstrip patch radiator they are pictured in Figs. 3 and 4 of the tutorial [4]. The presence of aperture coupling means that some portion of each element radiated power is distributed between all other elements in array behaving as receiving antennas. Hopefully, both types of mutual coupling are diminished as the normalized to wavelength inter-spacing between elements increases. Besides, proximity coupling being typically reactive by nature and a most significant part of total coupling drops much faster with distance than the aperture one. The rule of thumb tells us that the array radiators might be considered independent as long as the separation is above a wavelength as soon as the antenna array structure does not generate and support surface waves. These waves, if they exist, propagate inside the dielectric substrates and stay confined mainly within it causing undesired coupling that diminishes relatively slowly from element to element. One of the most

[3] At website httpdbook.com the reader can find extensive additional information, including ready to run CST MWS model files and Matlab scripts to extract and process CST simulation data. Click Blog and go to Mutual Coupling section for more results and comments. The raw text files of about 15GB (3D patterns and complex S-matrix) are available upon your request. Just click Contact at website top menu and fill up the message window.

effective ways to illuminate these waves is to use the thin dielectric substrate of ultra-low permittivity as we have done in the proposed model described below.

The term *grating lobes* means "… in-phase addition of a radiated field in more than one direction," i.e., the magnitude of grating lobes, unlike sidelobes, might reach the level of the main beam at some unwanted directions [7]. In a periodic array, i.e., an array with uniformly spaced and excited identical elements, a single grating lobe appearance is unavoidable as soon as the element spacing exceeds one-half wavelength but less than the wavelength. For example, the pattern of the linear array is free of grating lobes at the shortest designated wavelength λ_{min} until [4] $\sin\theta < 1/\left(\frac{d}{\lambda_{min}}\right) - 1$ where the scan angle is θ, d is the separation between adjacent radiators. Note that the deviations from uniformly spacing or the introduction of uncorrelated magnitude/phase error destroys the periodicity of an array and might help to suppress the grating lobe level [9]. But both topics are far from this paper scope. One of the most practical and effective ways to extend the scanning sectors or reduce the level of grating lobes is to change the array schematics moving, for example, each *even* row in Fig. 1 to the right at a distance equals to half of the array period as Fig. 2 exhibits. Loosely speaking, in such so-called triangular lattice, the elements in odd rows partially fill up the gap between elements in even rows and vice versa thereby reducing up to ~16% [9] the effective separation between array elements. Since the triangular lattice is the superposition of two rectangular as Fig. 3 indicates, the grating lobes are not eliminated entirely, but they are diminished in magnitude, shift to higher frequencies or a higher scan angle.

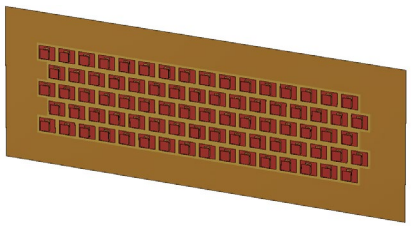

Figure 2. Schematics of Triangular Lattice

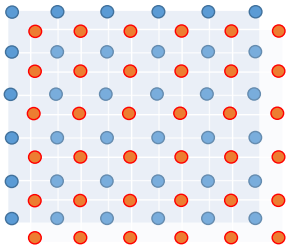

Figure 3. Triangular lattice as superposition of two rectangular

2. **Array Radiator.** To make relevant for practical applications the outcome of the following comparative analysis, a linear polarized (LP) back-fed stacked U-slot patch radiator (Fig. 4) optimized for 24 – 30 GHz band was chosen. It is compact, low profile, easy-to-integrate, lightweight, low cost, and quite simple to provide fast numerical simulation. The combination of two resonant components, a fed patch with a stacked element and U-slot, yields dual broadband characteristics [5] that are required in 5G systems with high data rate and low latency. The side arms of U-slot are symmetrically positioned with respect to the coax feed point shifted on 0.34

mm relative to the origin. The thin dielectric substrate of ultra-low permittivity of 1.07[4] assurances

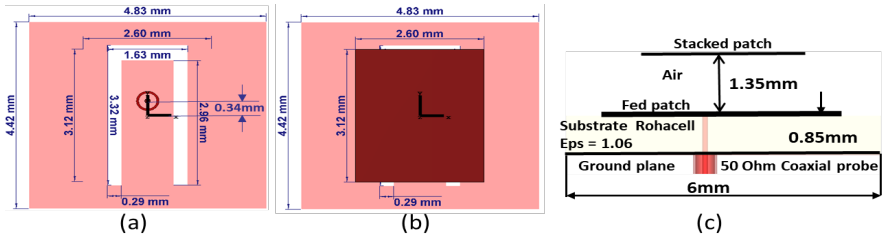

Figure 4. Element schematics. a) Top view of fed patch with U-slot, b) Top view fed and stacked patch, c) Side view.

the least possibility of surface waves. The stacked patch might be supported by a dielectric rod of small diameter (not shown in the drawing) or an additional layer of the same dielectric. The original cross-section sizes of radiator substrate and ground plane are 6x6mm or 0.48λ x 0.48λ at 24 GHz meaning no grating lobes at any scan angle while they are expected at 30 GHz where the element inter-spacing grows to 0.6λ x 0.6λ (see later).

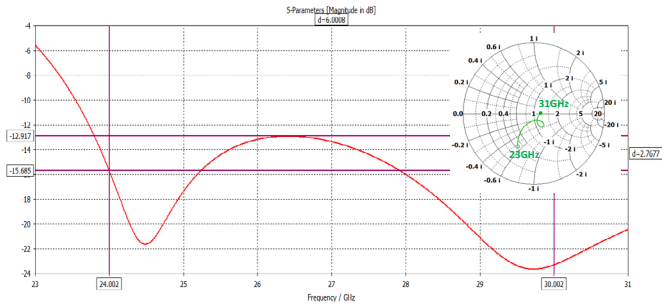

Figure 5. Return Loss and Input Impedance vs. frequency

The radiator model was developed using 3D full-wave CST MWS software and simulated in the time domain to get the wideband data over just one run. The frequency response is obtained through a Fast Fourier Transform (FFT) afterward. Since the time domain simulation is performed on a port-by-port basis, it takes less memory and faster as compared to the frequency domain. A ground plane of 31x31mm was added to alleviate the back radiation as well as ground edge diffraction. That is an extra 5 mm from each side and equals to half of the wavelength at 30 GHz. The plot of return loss, i.e., $20*\log_{10}(|S_{11}|)$, over frequency, is shown in Fig. 5 and demonstrates the excellent wideband performance with the return loss below -12 dB at all desired frequencies. The enclosed Smith chart reflects the corresponding input impedance. As expected, both plots indicate the presence of two overlapping resonances, the first at 24.47 GHz and the second one at 29.62 GHz making the radiator similar to Chebyshev

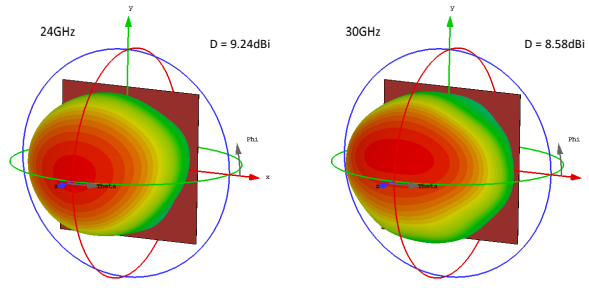

Figure 6. Patterns with extended ground

[4] For example, ROHACELL® 51 IG/A with tan δ = 0.0037 that can are foamed into a finished core in a mold with all patches directly integrated during the foaming process. See https://www.rohacell.com/sites/lists/re/documentshp/rohacell-dielectric-properties-en.pdf and https://www.rohacell.com/product/rohacell/en/downloads/press-releases/pages/article.aspx?articleId=101326.

filter of 2nd order. Since the reactive energy stored in E- and H-fields typically reaches extreme around resonances [6], this element is expected to have a spike of spatial proximity coupling around these frequencies. Fig. 6 depicts 3D element patterns and its directivity [dBi] at two frequencies, 24 GHz and 30 GHz.

Note that the directivity at both frequencies is not directly related to element geometrical size of 6x6mm. It means that the effective radiation area [6] is much broader than this physical area. It happened since the nearby and responsible for far-field radiation EM fields extend far beyond of 6x6mm.

3. Infinite periodic array environment. The Floquet-Bloch theory lets deduce the property of the whole array with mutual coupling included from a simulation of just single unit cell as soon as the certain periodic boundary conditions (on surfaces in blue) are established as Fig. 7 depicts. Behind this approach lies the assumption that all array elements are uniformly excited, identical in their behavior, and placed into the nodes of a planar and uniform grid of infinite extent, i.e., they form an ideal infinite 2D periodic structure. Typically, such an approach works perfectly well just for large arrays of a thousand or more elements, but it is worth to check its applicability for arrays of smaller sizes. The main disadvantage of such approach is that the information about the element active impedance and level of mutual coupling is lost. Term "active impedance" is defined as the input impedance of some element when only this element in the array is driven, and all others are terminated with matched loads. The remarkable fact is that the knowledge of active impedance is precious, letting reconstruct the patterns of driven element and whole array [8].

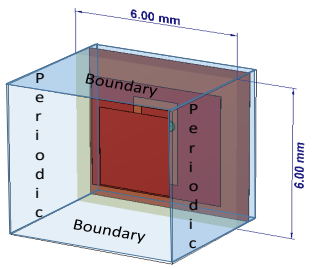

Figure 7. Element schematic in infinite-array environment

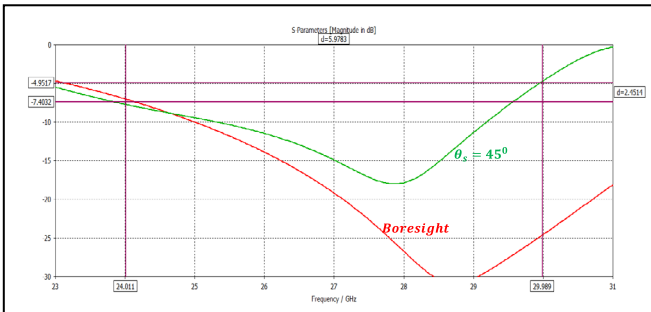

Figure 8. Return loss vs. frequency

Fig.8 represents the graph of return loss for two beam positions, boresight (red line) and $\theta_{scan} = 45°$. Both curves reflect the parameters of every element in the array as long as all elements are driven and demonstrate quite satisfactory broadband performance. The comparison of plots in Figs.3 and 6 clearly shows the impact and importance of mutual coupling. The patterns in Fig.9 are reasonably similar in shape to shown in Fig.6, but the directivities are different. Mention only that the element directivity is defined by the magnitude and phase distribution of E-

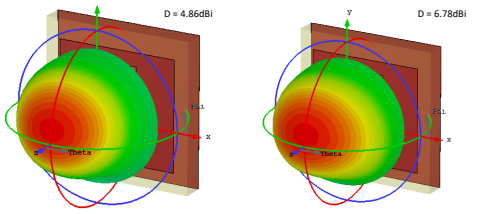

Figure 9. Infinite-array environment patterns

and H-field not only over of the element aperture but its *vicinity* and could be characterized so-called effective aperture [6, 7]. In case of a single element in free space (see Fig.4), the effective aperture exceeds its physical sizes because the fields cover a larger area than its physical sizes (look again at Figs. 3 and 4 of the tutorial [4]). In the case of the element in the infinity array, the effective aperture of the element in Fig.7 is almost equal to its cell, i.e., physical sizes of the element.

4. **Full-wave Simulation of 5x16 Array in Fig.1**. The last resort is the numerical simulation of the whole array using one of commercial 3D full-wave software like CST MWS, HFSS, COMSOL, EMPIRE XPU, etc., or to get all data through testing inside antenna range. Thereby it can be generated an embedded database of 3D patterns and scattering (S-matrix) or impedance Z/Y-matrix for each element in the array. This tactics leads evidently to massive outcome database (see the footnote[1] above) and assumes access to high-performance computers. The implemented parallel processing, as well as GPU and cache accelerating [6], are desired. All following data of numerical simulation were obtained using CST MWS.

Let's start from the element active directivity [in dBi] patterns of elements belonging the 5x16 panel in Fig.1. Remind that the active means a single array element is driven while all others are connected to dummy loads. The set of plots in Fig.10a and 10b presents the patterns of all 80

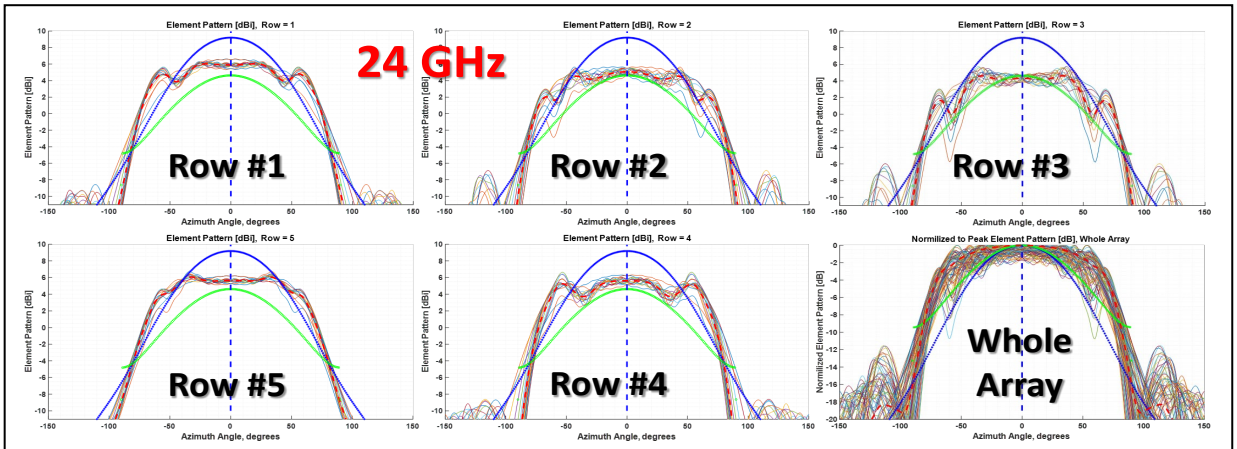

Figure 10a. Active patterns of 5x16 array in rectangular lattice

elements split into the raw groups at 24 GHz and 30 GHz, respectively. The red dotted line shows the averaged pattern for each row. For comparison, the azimuthal cut of pattern depicts in Fig.6 marked by a blue asterisk symbol. The green line formed by circle markers reflects the azimuthal cut of pattern in Fig.9. Note that the latter is not an active pattern because the element and an infinite number of its neighbors are driven uniformly. As expected, in the angular sector $\pm 45°$ the element patterns in the rim as well as next-to-rim rows practically identical. The set of curves titled as whole array (the bottom right corner) presents all 80 patterns being normalized to their peak to demonstrate the patterns' shape and evaluate the array beam steering performance. The steepest pattern envelope at 24 GHz describes the no-mutual-coupling element while the infinite-array element is closed in its shape to the active pattern. If so, we can expect the overestimated scan loss relative to theoretical level $10*\log_{10}(\cos\theta_{scan})$ [6] with the no-mutual-coupling array numerical model. Apparently, at 30 GHz the infinite-array simulation should be overoptimistic. A closer

look at the active patterns brings out that the patterns are not only different but mainly asymmetrical relative to $\theta = 0$. The expected consequence is the slim asymmetry in scan loss as

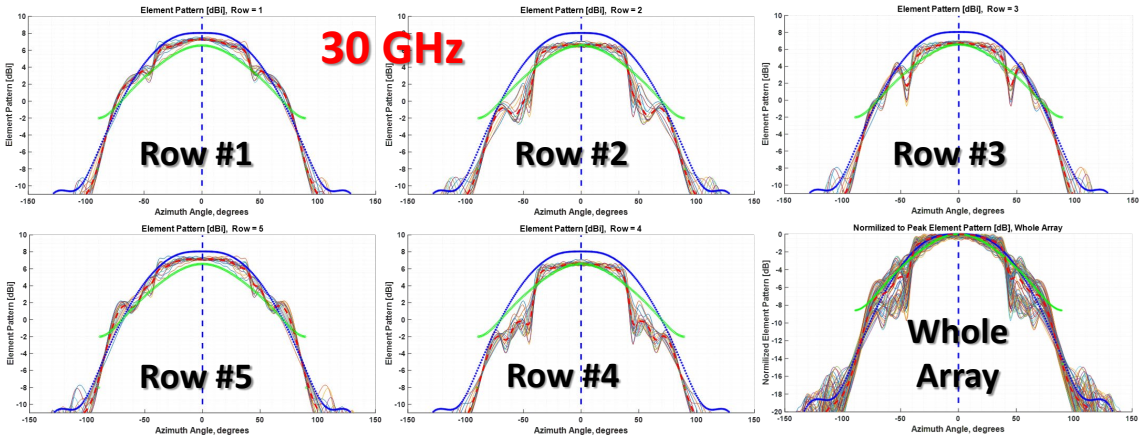

Figure 10b. Active patterns of 5x16 array in rectangular lattice

The main beam is steered to $+\theta_{scan}$ or $-\theta_{scan}$. Besides, the beams slightly squint to the right or left with the ripples, droops, and overshoots on the top. All such terminology is typical for the analysis of square wave passing low-band filter. This similarity is not occasional because both the

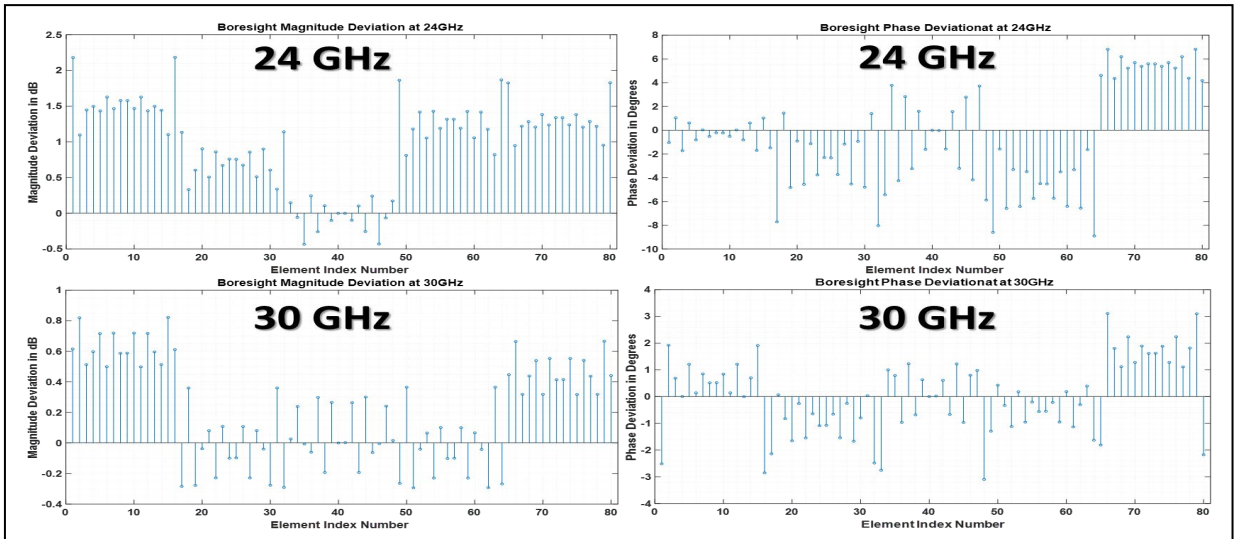

Figure 11. Deviation of boresight active directivity and phase vs. element index number

pattern and signal envelope are defined formally by very close in structure Fourier and so-called Fourier-Floquet series. The pattern envelopes can be described by the set of spatial harmonics while the signal processing is based on alike series in the frequency domain. It means a finite periodic array is somehow equivalent to a low-band filter "cutoffing" the radiation of high order spatial harmonics and keeping them nearby in the form of reactive fields. Such analogy lets not only control the numerical simulation process but often predict its outcome without any simulation. The stem plots in Fig.11 reflect the deviation of boresight active directivity (two left plots) from the peak vs. the element position in the array. Such differences can reach -2.5 dB at 24 GHz and diminish to -0.8 dB at 30 GHz. Finally, notice that the pattern variations are more noticeable at 24

GHz frequency nearby to the lowest resonance because of strong proximity coupling. A couple of plots to the right tells us that the phase of boresight radiation slightly varies too within a few degrees. *Therefore, to avoid the antenna performance degradation, an internal diagnostic and calibration system should be implemented.*

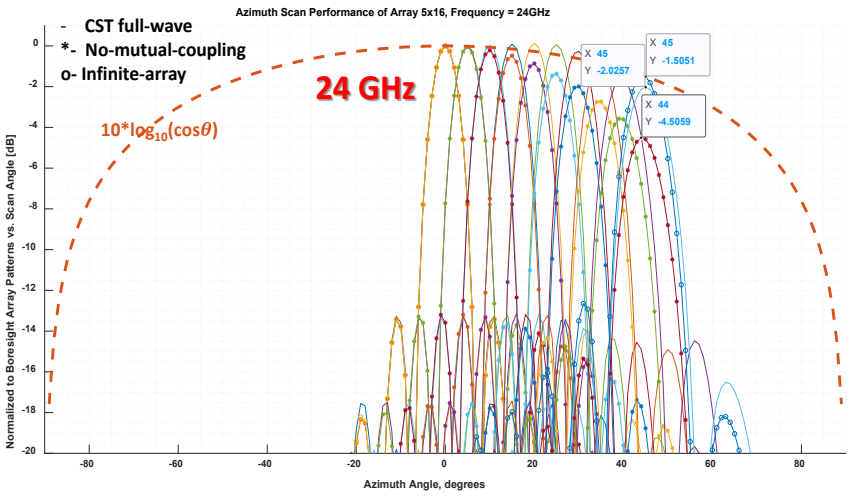

Figure 12a. Normalized to boresight beam steering performance

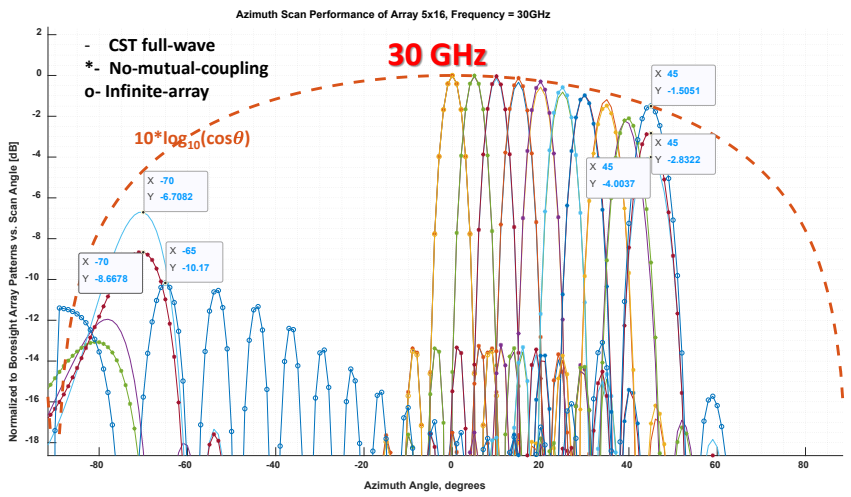

Figure 12b. Normalized to boresight beam steering performance

The graphs in Fig.12a and 12b demonstrate the normalized to boresight beam steering up to 45° in azimuth at 24 GHz and 30 GHz, correspondingly. As predicted, there is no grating lobe at 24 GHz. The full-wave simulation gives -2.02dB scan loss while the no-mutual-coupling and infinite-array approach are -4.50 dB and -1.50, respectively. At 30 GHz these numbers are -4.00 dB, -2.83 dB, and -1.50 dB, accordingly. Two latest results are too optimistic. There is the same situation with the prediction of the grating lobe level. The full-wave, no-mutual-coupling, and infinite-array approach predicts -2.71 dB, -1.83 dB, and -8.67 dB relative to the peak at $\theta_{scan} = 45°$. The infinite-array number is certainly too good to believe. Therefore, *the correctness of scan loss and grating lobe level should be checked through the full-wave simulation.*

5. **Boresight Return Loss and Input Impedance**. Fig.13 depicts the return loss in dB of all 80 elements are driven uniformly in magnitude and phase to form the boresight beam. As predictable from the array symmetry, there are 3 sets of curves with comparable frequency dependency; row 1 and 5 (light blue oval) including mostly the rim elements, row 2 and 4 (light green oval) including

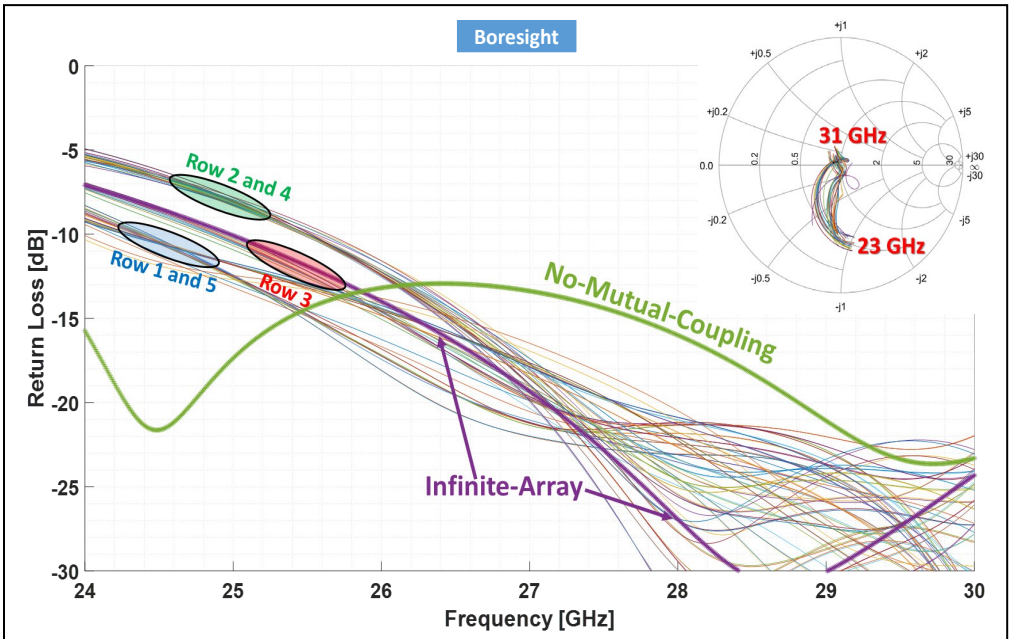

Figure 13. Return loss and impedance of elements driven uniformly

mostly the next-to-rim elements, and row 3 (light red oval) including the center elements. The solid grin line is put for comparison and shows that the disregard of mutual coupling leads to the wrong results. The infinite-array approach is much better. As expected, this curve follows closely to the center elements only while reflects the frequency behavior of rim and near-rim elements purely. The enclosed Smith chart reveals the input impedance (normalized to 50 Ohms). That is an important hint. *The database of the consistent model platform should include the digital images of as minimum 3 essential elements: one from the rim, one from next-to-rim, and the last from center elements.*

6. **Full-wave Simulation of 5x16 Array with Triangular Lattice in Fig.2**. The reader can find more detailed data about this geometry going to website https://emfieldbook.com**.** Present just several substantial results. The active pattern deviations become more noticeable not only from element to element but from row to row. The same is correct for the active return loss. In spite of it, the input impedances of elements of boresight radiating array continue to be well collimated around the

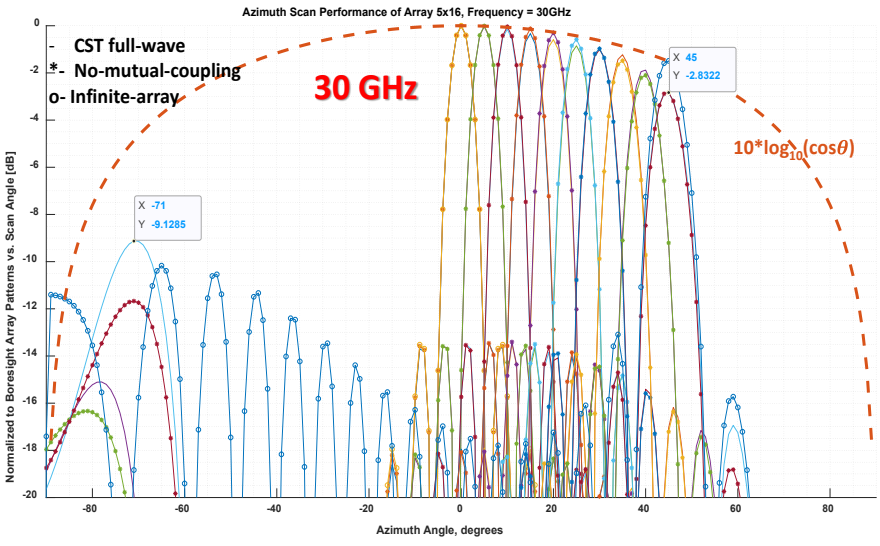

Figure 14. Normalized to boresight beam steering performance

center of Smith chart. The grating lobe according to graphs in Fig. 14 drops to -6.3 dB as the beam is steered to 45° at 30 GHz. It is not a very significant reduction, but that turns out to be enough for the scan loss diminishes to -2.83 dB. This is primarily explained by the fact that the element active patterns become slightly wider in triangular lattice vs. rectangular. Notice the increase in sidelobe level relative to rectangular lattice. For more details and comments, visit https://emfieldbook.com.

Conclusions. Now we possess all essentials to compare the results using different approaches: no-mutual-coupling, infinite-array environment, and full-wave CST simulation of the array in a triangular and rectangular lattice. All data about directivity, scan loss, and grating lobe level (column 5, beyond the slash symbol) are summarized in Table 1. Bringing up the data from Fig.11 we can come to conclusions:

Table 1

AZ Scan Angle	Boresight		45degrees		Scan Loss at 45 degrees	
Frequency	24GHz	30GHz	24GHz	30GHz	24GHz	30GHZ
No-Mutual-Coupling	24.2dBi	25.8dBi	22.6dBi	22.3dBi/-5.8dB	-1.6dB	-3.5dB
Infinite-Array	23.7dBi	25.6dBi	22.2dBi	24.1dBi/-8.7dB	-1.5dB	-1.5dB
Finite Rectangular	24.0dBi	25.8dBi	22.5dBi	21.3dBi/-2.3dB	-1.5dB	-4.5dB
Finite Triangular	24.1dBi	25.8dBi	22.8dBi	23.0dBi/-6.3dB	-1.3dB	-2.83dB

1. Any model can be used to obtain the practically correct estimation of boresight directivity.
2. As minimum 3 different elements (rim, near-rim, and center) must be taken into consideration to reach the accurate estimation of scan performance, especially for the wideband array at a higher end of the frequency band.
3. The scan and grating lobe performance of an array in triangular lattice generally requires the full-wave examination.
4. As a rule of thumb, the scan loss/input impedance vs. frequency requires the full-wave analysis. Some rough estimation might be obtained using the infinite-array environment model, but that issue needs additional investigation.

Acknowledgment. This work has been encouraged by Victoria Pereira, President of Otava, Inc., and partially funded by her company.

REFERENCES:

1. David Vye and Jack Browne, "Platform Propels RF Designs from Concepts to Products," *Microwave & RF,* October 2018, pp. 62 – 63.
2. Jack Browne, "Bringing mmWave Signals to the Masses,' *Microwave & RF,* June 2019, pp. 51 – 54, 68.
3. Sarah Yost, "First to 5G: Who Will Win?" *Microwave & RF,* June 2019, pp. 35 – 36.
4. Kenneth Puglia, "A Brief Tutorial on Microstrip Antennas (Part 1)," *Microwave & RF,* November 2018, pp. 40 – 62.

5. J.A. Anasari and R. B. Ram, “Broadband Stacked U-slot Microstrip Patch Antenna,” *Progress In Electromagnetics Research Letters*, Vol. 4, pp. 17–24, 2008
6. Vladimir Volman and Andrzej Jeziorski, Engineering Electrodynamics. House of Maxwell’s Electrodynamics, 2017.
7. Constantine A. Balanis, Antenna Theory, 3rd Edition, Wiley & Son, 2005.
8. David M. Pozar, “A Relation between the Active Input Impedance and the Active Element Pattern of a Phased Array,” *IEEE Transactions on Antennas and Propagation*, vol. 51, No. 9, September 2003, pp. 2486 – 2489, or visit website
https://pdfs.semanticscholar.org/4f10/5bda3300308e7771276cf65b6557419f2e1d.pdf
9. John S. Williams, ”Electronic Array Design,” *Tutorial*, visit website
https://intranet.birmingham.ac.uk/eps/documents/public/emuw2/SCF01.pdf